Applied Catalysis B: Environmental 164 (2015) 192–203

Contents lists available at ScienceDirect

Applied Catalysis B: Environmental

journal homepage: www.elsevier.com/locate/apcatb

Oil-in-water self-assembled Ag@AgCl QDs sensitized Bi_2WO_6: Enhanced photocatalytic degradation under visible light irradiation

Yinghua Liang, Shuanglong Lin, Li Liu, Jinshan Hu, Wenquan Cui*

College of Chemical Engineering, Hebei United University, No. 46, Xinhua West Street, Tangshan 063009, PR China

ARTICLE INFO

Article history:
Received 11 June 2014
Received in revised form 20 August 2014
Accepted 30 August 2014
Available online 19 September 2014

Keywords:
Quantum dots
Oil-in-water self-assembly
Ag@AgCl/Bi_2WO_6
Photocatalytic
Degradation

ABSTRACT

Quantum dots (QDs) Ag@AgCl decorated on the surface of flower-like Bi_2WO_6 (hereafter designated Ag@AgCl/Bi_2WO_6) were prepared via a facile oil-in-water self-assembly method. The photocatalysts were characterized by X-ray diffraction (XRD), Scanning electron microscopy (SEM), Transmission electron microscopy (TEM), UV–vis diffuse reflectance spectroscopy (DRS) and X-ray fluorescence spectrometer (XRF) etc. The characterization results indicated that QDs Ag@AgCl was observed to be evenly dispersed on the surface of Bi_2WO_6, and was approximately 10–20 nm in size. Ag@AgCl/Bi_2WO_6 composites exhibited excellent UV–vis absorption, due to quantum dimension effect of Ag@AgCl QDs, the surface plasmonic resonance (SPR) of Ag nanoparticles and the special flower-like structure of Bi_2WO_6. The photo-electrochemical measurement verified that the suitable band potential of Ag@AgCl and Bi_2WO_6 and the existence of metal Ag resulted in the high efficiency in charge separation of the composite. The photocatalytic activities of the Ag@AgCl/Bi_2WO_6 samples were examined under visible light irradiation for the degradation of Rhodamine B (RhB). The composite presented excellent photocatalytic activity due to the synergetic effect of Bi_2WO_6, AgCl, and Ag nanoparticles. The Ag@AgCl(20 wt.%)/Bi_2WO_6 sample exhibited the best photocatalytic activity, degrading 97.61% RhB after irradiation for 2 h, which was, respectively, 1.33 times and 1.32 times higher than that of Ag@AgCl and Bi_2WO_6 photocatalyst. Meanwhile, phenol was degraded to further prove the degradation ability of Ag@AgCl/Bi_2WO_6. Additionally, studies performed using radical scavengers indicated that $O_2^{-}\cdot$, h^+ and Cl^0 acted as the main reactive species. Based on above, a photocatalytic mechanism for organics degradation over Ag@AgCl/Bi_2WO_6 was proposed.

1. Introduction

The semiconductor photocatalysis using solar energy has been recognized as one of the most effective strategies to solve water pollution problems by decomposing pollutants and disinfection [1,2]. Although remarkable progress has been made in TiO_2-based photocatalyst, such as doping metals [3], coupling with other semiconductors [4–6], and anchoring organic dyes [7], to overcome its drawbacks of wide band gap, rapid recombination of photo-generated electrons and holes, TiO_2-based photocatalyst still cannot totally meet the requirement of practical application in environmental cleaning driven by solar energy. Therefore, the development of new and more efficient visible-light-driven (VLD) photocatalysts has been still an urgent topic in the viewpoint of using solar energy [8].

Previous reports revealed that silver@silver halide [9] (Ag@AgX (X = Cl, Br, I)) photocatalysts possess excellent visible light driven photocatalytic degradation of organic pollutants and disinfection due to the localized surface plasmon resonance (SPR) effect exhibited by Ag nanoparticles (NPs). Importantly, recent works have led to the development of Ag@AgX-based composite photocatalysts with the advantages of efficient visible light absorption, low cost, and relative stability. For example, it has been reported that Ag@AgCl/WO_3 [10], Ag@AgCl/MCM-41 [11], Ag@AgCl/TiO_2 [12], Ag@AgI/Al_2O_3 [13], Ag@AgCl/GO [14] and AgI/TiO_2 [15] showed enhanced visible light photocatalytic degradation and disinfection. Furthermore, Ag@AgX were successfully recombined with the flower-like semiconductors, such as Bi_2WO_6 [8] and BiOBr [16], and the photocatalytic activity were greatly improved by the synergy effect of SPR effect driving from Ag NPs and light scattering effect driving from flower-like structure. These new composite photocatalysts greatly improved the large scale practical application in the utilization of solar energy and provide new strategies to develop VLD photocatalysts. However, the bulk phase recombination of Ag@AgX with semiconductors could lead to the

* Corresponding author. Tel.: +86 315 2592169; fax: +86 315 2592169.
E-mail address: wkcui@163.com (W. Cui).

http://dx.doi.org/10.1016/j.apcatb.2014.08.048
0926-3373/

serious aggregation and poor dispersity, resulting in the decrease of specific surface area and covering the active sites.

On the other hand, the decoration of quantum dots (QDs) semiconductors, such as CdS [17], CdSe [18], on the host semiconductors was regarded as the efficient way to enhance the light conversion efficiency, because of the large surface area, quantum confined effect, close-contacted interface, and less aggregation, which are able to harvest more visible light and improving the photo-induced charge separation [19]. Meanwhile, different from the rod or spherical shaped nanostructure, the flower-like Bi_2WO_6 photocatalysts have attracted much attention because of their large surface areas, plenty of meso-pores with ordered open pore frameworks, within which the flower-like photocatalysts can effectively harvest visible light due to multiple scattering [20]. Moreover, it is considered that the large surface areas and ultrathin thick nano-plate of the flower-like structure could decrease the recombination efficiency of the photo-excited electron–hole pairs and favor their transfer to the surface to react with organic pollutants [21]. However, to the best of our knowledge, QDs Ag@AgCl sensitized novel flower-like Bi_2WO_6 photocatalysts have not reported yet. Therefore, it is necessary to design a novel photocatalyst with QDs Ag@AgCl and Bi_2WO_6, which possess superior activity under visible light.

In the present work, the photocatalysts of QDs Ag@AgCl-decorated flower-like Bi_2WO_6 (hereafter designed as QDs Ag@AgCl/Bi_2WO_6) were successfully fabricated via a multistep route, in which a hydrothermal precipitation was employed to synthesize flower-like Bi_2WO_6 and an oil-in-water self-assembly (water/oil) synthesis was used to deposit AgCl on Bi_2WO_6, and UV light reduction was addressed to form Ag NPs. The obtained samples were investigated by means of scanning electron microscopy (SEM), transmission electron microscopy (TEM), X-ray diffraction (XRD), and UV–vis diffuse reflectance spectroscopy (DRS) etc. The photocatalytic degradation activities of QDs Ag@AgCl/Bi_2WO_6 were performed using Rhodamine B (RhB) dye and phenol as the model molecular. The results showed that QDs Ag@AgCl was observed to be evenly dispersed on the surface of flower-like Bi_2WO_6, and was approximately 10 nm in size; the prepared Ag@AgCl/Bi_2WO_6 samples possessed enhanced optical absorption from 420 to 700 nm; The Ag@AgCl(20 wt.%)/Bi_2WO_6 sample exhibited the best photocatalytic activity, degrading 97.61% RhB after irradiation for 2 h. The improvement of photocatalytic activity is because of the increased surface area, tight interface contact which could improve the photo-induced charge separation.

2. Experimental

2.1. Photocatalyst synthesis

All of the reagents used were analytical grade and used without further purification. In a typical synthesis of Bi_2WO_6, a defined amount $Bi(NO_3)_3{\cdot}5H_2O$ and $Na_2WO_4{\cdot}2H_2O$ was initially dissolved in 80 mL deionized water under magnetic stirring at room temperature. After 40 min, the slurry solution was transferred into a 90 mL Teflon-lined autoclave and subsequently heated at 180 °C for 12 h. The reactor was then allowed to cool to room temperature naturally. The yellow precipitate was collected and washed with distilled water, and the final products dried at 80 °C for 8 h.

Ag@AgCl/Bi_2WO_6 was prepared via an oil-in-water self-assembly method. Bi_2WO_6 powder, NaOH, and $AgNO_3$ were dissolved into deionized water and a certain amount of carbon tetrachloride (CTAC) solution was added dropwise at room temperature under vigorous magnetic stirring for 20 min. After the CTAC addition, the reaction mixture was magnetically stirred for another 20 min to evaporate the chloroform solvent. The resulting suspension was then filtered, and washed with deionized water and ethanol, respectively. The obtained AgCl/Bi_2WO_6 powder was dispersed in distilled water, and irradiated with a 250 W metal halide lamp (Philips), equipped with wavelength cutoff filters for $\lambda \geq 420$ nm. The resulting sample (Ag@AgCl/Bi_2WO_6) was washed with distilled water and anhydrous ethanol to remove the surfactant, and the final products (hereafter designated Ag@AgCl/Bi_2WO_6) were dried at 80 °C for 8 h in the dark.

For comparison, an Ag@AgCl/Bi_2WO_6 sample was prepared via a precipitation method with Bi_2WO_6 powder, NaOH, $AgNO_3$ and CTAC, and the as-prepared catalyst was denoted as P-Ag@AgCl/Bi_2WO_6.

Pure Ag@AgCl was synthesized similarly using an oil-in-water self-assembly method with $AgNO_3$, and CTAC.

2.2. Photocatalyst characterization

The crystal structures and phase data for the prepared samples were determined by X-ray diffractometry (XRD) using a Rigaku D/MAX2500 PC diffractometer with Cu $K\alpha$ radiation, with an operating voltage of 40 kV and an operating current of 100 mA. The morphology of the samples was investigated by scanning electron microscope (SEM) (Hitachi, s-4800) and energy dispersive X-ray spectroscopy (EDX), as well as by transmission electron microscopy (TEM) (JEOL Ltd., JEM-2010). UV–vis light (UV–vis) diffuse reflectance spectra were recorded on a UV–vis spectrometer (Puxi, UV1901). The chemical compositions of the samples were tested by an X-ray fluorescence spectrometer (XRF, Rigaku, ZSX Promusll). Surface areas of the samples were determined using Brunauer–Emmett–Teller (BET) method based on the N_2 adsorption and desorption isotherms collected on a Quantachrome Nova 4200e automatic analyzer (USA). The chemical states of the photocatalysts were analyzed by X-ray photoelectron spectroscopy (XPS) using a XSAM800 apparatus. The time-resolved PL was performed on a Fluorescence and phosphorescence lifetime and steady-state spectrometer (Edinburgh instruments FLSP920, LED 360 nm). Electrochemical and photo-electrochemical measurements were performed in a constructed three electrode quartz cell system. Pt sheet was used as a counter electrode and Hg/Hg_2Cl_2/sat. KCl was used as reference electrodes, while the thin film on indium–tin oxide (ITO) was used as the working electrode for investigation. The photoelectrochemical experimental results were recorded with a CHI 660B electrochemical system.

2.3. Photocatalytic activity

The photocatalytic activities of Ag@AgCl/Bi_2WO_6 composites were evaluated by the degradation of RhB under irradiation of visible light. For the first series of tests, a 250 W halide lamp (Philips) with a 420 nm cutoff filter was used at a distance of 10 cm from an unsealed beaker. In the second series of tests, a glass reactor with circulating water flowing outside to control the temperature to 25 ± 2 °C was employed. For each test, 0.25 g catalyst powder was added into 250 mL RhB solution. Prior to irradiation, the test solution was stirred in the dark for 30 min. During irradiation, a 3 mL sample of the reaction suspension was withdrawn every 15 min, centrifuged at 10,000 rpm for 6 min to remove the particles, and the collected supernatant solutions were analyzed by a UV–vis spectrophotometer.

The degradation efficiency (%) was calculated as follows:

$$\text{degration}\,(\%) = \frac{C_0 - C}{C_0} \times 100\% \quad (1)$$

where C_0 is the initial concentration of RhB, and C is the RhB concentration at time t.

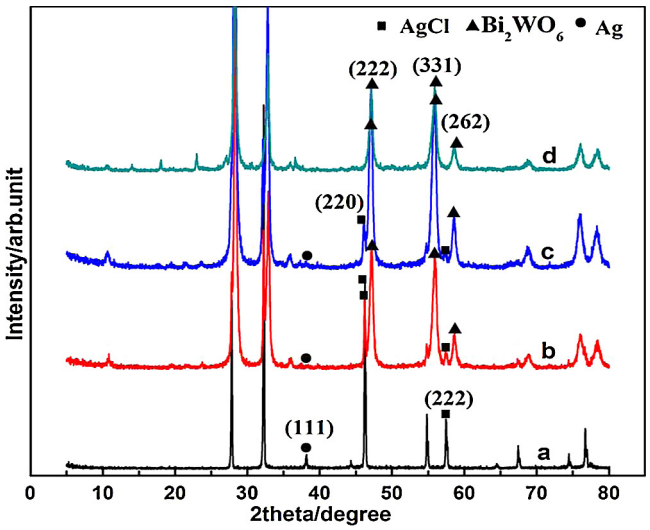

Fig. 1. XRD patterns of photocatalysts: (a) Ag@AgCl, (b) Ag@AgCl (20 wt.%)/Bi_2WO_6, (c) Ag@AgCl (5 wt.%)/Bi_2WO_6, (d) Bi_2WO_6, respectively.

Photocatalytic activities for RhB in the dark in the presence of the photocatalyst and under visible-light irradiation in the absence of the photocatalyst were also evaluated.

Additionally, the degradation procedure of phenol was the same as that of RhB.

3. Result and discussion

3.1. Catalyst characterization

The typical XRD patterns obtained from the Ag@AgCl, Bi_2WO_6 and the Ag@AgCl/Bi_2WO_6 composites prepared with different contents of Ag@AgCl are shown in Fig. 1. The Ag@AgCl was found to be mainly composed of the chlorargyrite AgCl phase, and all of the peaks matched with the JCPDS standard data for AgCl (JCPDS card no. 31-1238). The diffraction peaks obtained were intense and sharp, indicating that the obtained Ag@AgCl photocatalysts were well crystallized. As shown in Fig. 1, the characteristic diffraction peaks for AgCl at 2θ of 46.2°, and 57.5° were attributed to the (2 2 0), and (2 2 2) crystal planes of AgCl, while the peaks at 38.2° was attributed to the small quantity of Ag which formed. The diffraction peaks observed in the spectra for Bi_2WO_6 and the as-prepared Ag@AgCl/Bi_2WO_6 appearing at 2θ values of 48.5°, 55.8° and 58.5° were assigned to (2 2 2), (3 3 1) and (2 6 2) crystal planes of rhombic Bi_2WO_6 (JCPDS39-0256). In addition, the calculated d values did not change and corresponded to 1.875, 1.646 and 1.576 nm, indicating that the flower structure of Bi_2WO_6 was not significantly altered upon introduction of QDs Ag@AgCl [22]. No other diffraction peaks attributed to Ag were detected in the patterns, because the content of Ag contained in the composites was thought to be below the detection limit of the apparatus.

The morphology, crystal structure and composition of the products were detected by SEM, TEM, SAED and EDX, respectively. As shown in Fig. 2, the morphologies of Bi_2WO_6, pure Ag@AgCl and Ag@AgCl/Bi_2WO_6 were observed using SEM and TEM. The SEM image of Bi_2WO_6 is shown in Fig. 2a, and was seen to possess flower-like superstructures with diameters of approximately 3 μm, built from two-dimensional nanoplates with a smooth surface (as seen in the inset of Fig. 2a). The pure Ag@AgCl was observed as shown in Fig. 2b, and its morphology was comprised of irregular spherical particles of about 50–100 nm. The sample containing Ag@AgCl deposited onto Bi_2WO_6 prepared by self-assembly method is shown in Fig. 3c, with the equivalent sample prepared by the precipitation method shown in Fig. 3d for comparison. The shape of Bi_2WO_6 did not change upon QDs Ag@AgCl-loading, which indicated that the QDs Ag@AgCl deposition process did not damage its flower-like structure. In addition, Ag@AgCl-loading could well promote the scatter of Ag@AgCl, and reduce its grain size. From Fig. 3c, some spherical particles with a size range of from 5 to 20 nm were observed to be uniformly deposited on the surface of Bi_2WO_6, indicating the increase of the surface roughness of the flower-like structure [23]. The BET results revealed that the specific surface area of Ag@AgCl/Bi_2WO_6 (12.07 m^2/g) nano-composite was larger than that of pure Bi_2WO_6 (7.22 m^2/g) (as shown in Table 1) and the light absorption was considered to be enhanced due to the increased light scattering. From Fig. 3d, the particle size of P-Ag@AgCl/Bi_2WO_6, which was synthesized via precipitation method was seen to be around 0.4 μm, and the aggregation of Ag@AgCl was observed to be significant compared to Fig. 3c. Interestingly, nanoparticles with a size range from 5 to 20 nm were dispersed on the surface of the Bi_2WO_6, and were thought to be form nanojunctions [8], as shown in TEM image (Fig. 3e). The HR-TEM image (Fig. 3f) of the sample indicated the lattice spacing of Ag, AgCl and Bi_2WO_6, and were determined to be 0.24, 0.28 and 0.45 nm, are in good agreement with the crystal planes for the (1 1 1), (2 0 0) and (0 2 1) faces, respectively. The Bi_2WO_6 was also observed to be partially enwrapped in an amorphous nano-shell, where the AgCl crystal is located beside it. The SAED pattern collected from Ag@AgCl/Bi_2WO_6 is shown in Fig. 3g, and polycrystalline diffraction rings could be observed. This EDX elemental mapping was performed on a single microsphere in the images, and the corresponding EDX spectrum of the Ag@AgCl/Bi_2WO_6 composite is shown in Fig. 3h. Peaks attributed to Ag, Cl, Bi, W and O were observed, which were indicative of the Ag, AgCl, and Bi_2WO_6 components present in the system. In addition, the elemental composition of the composite nameplates was further analyzed by XRF. The result is shown in Table 2, and the atomic ratio of Ag to Cl was found to be 1.4:1, indicating the presence of Ag in Ag@AgCl nanojunction system. Based on the XRF results, the atomic ratio of Bi to W to O was found to be 1.9:1:7.3, which was less than the theoretical ratio of 2:1:6 expected from Bi_2WO_6. Since the percentage of O was higher in the experimental sample than in the theoretical ratio for Bi_2WO_6, H_2O was thought to possibly be present in the prepared Ag@AgCl/Bi_2WO_6 composite.

On the basis of the above analysis, a possible formation mechanism of the Ag@AgCl/Bi_2WO_6 was proposed, as shown in Fig. 3. When Ag^+ was added into the reaction system, the Ag^+ ion was thought to interact electrostatically with Bi_2WO_6 to form Ag^+–Bi_2WO_6 complexes in the aqueous system. In the following process, these adsorbed Ag^+–Bi_2WO_6 complexes reacted with the CTAC to form the AgCl in situ on the surface of Bi_2WO_6. In the typical synthesis, a certain amount of Bi_2WO_6 and $AgNO_3$ were successively added to distilled water to form the host solution, and the guest liquid phase of CTAC in distilled water was then injected into the solution. In this oil/water system, the Ag^+ dispersed in aqueous solution uniformly, and the hydrophobic alkyl chains of CTAC dissolved and pointed toward the core of the nanosized chloroform phase with the polar headgroup ($-N(CH_3)_3^+$), and the counterion (Cl^-) dissolved and pointed toward the host water phase [24]. AgCl nanospecies were generated immediately when Ag^+ and Cl^- collided, and the reaction was thought to progress predominantly at the outer surface of the nanosized oil phase. Simultaneously, some of the Ag^+ cations were in situ converted into metallic Ag^0 species by the ambient light, leading to the formation of Ag@AgCl nanostructures. In this system, the Ag element of the target products originated from the host water phase, which surrounded the guest oil droplets, while the Cl component originated from the guest oil phase, which was dispersed in the host water phase. As a consequence, the surface of the formed AgCl nanostructures was thought

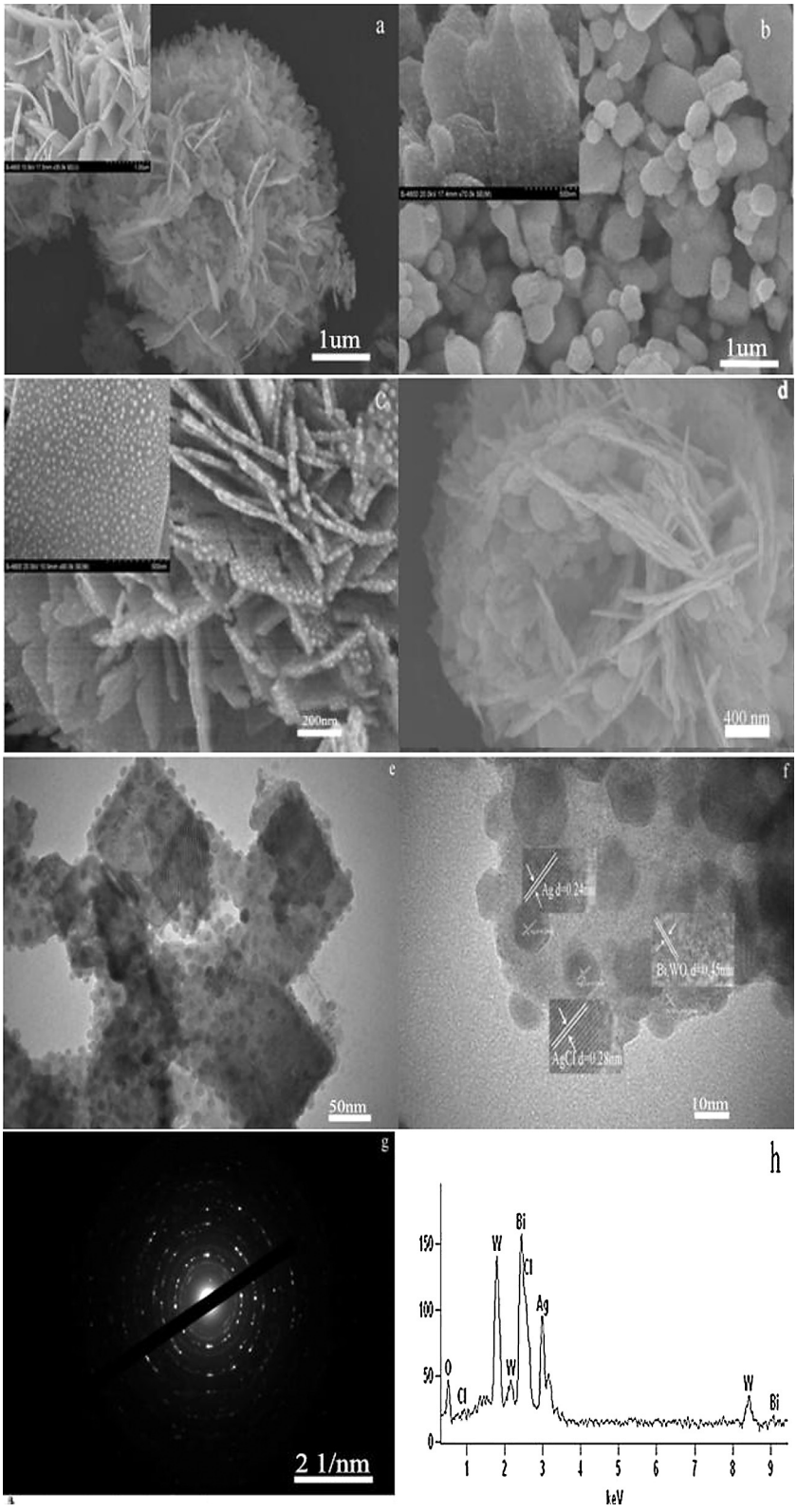

Fig. 2. SEM images of prepared photocatalysts: (a) Bi_2WO_6, (b) Ag@AgCl, (c) Ag@AgCl/Bi_2WO_6, (d) P-Ag@AgCl/Bi_2WO_6, (e) TEM images of (c) Ag@AgCl/Bi_2WO_6, (f) HRTEM images of (c) Ag@AgCl/Bi_2WO_6, (g) SAED pattern of (c) Ag@AgCl/Bi_2WO_6 and (h) corresponding EDX pattern of (c).

Table 1
Specific surface area of Ag@AgCl/Bi_2WO_6 composite catalysts.

Photocatalysts	Bi_2WO_6	Ag@AgCl(5 wt.)/Bi_2WO_6	Ag@AgCl(20 wt.)/Bi_2WO_6	Ag@AgCl(25 wt.)/Bi_2WO_6
Surface area [m^2/g]	7.22	9.13	12.07	14.23

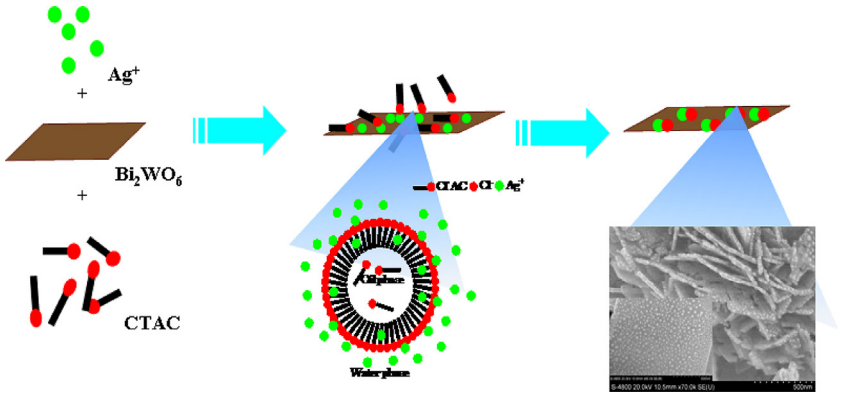

Fig. 3. Mechanism of formation of Ag@AgCl/Bi_2WO_6 sample.

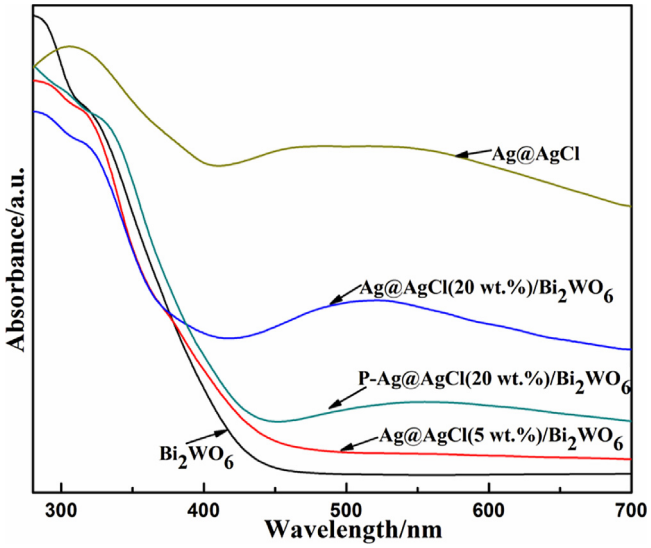

Fig. 4. UV–vis diffuse reflectance spectra of prepared photocatalysts.

to be primarily terminated by and thus relatively enriched with Ag, resulting in a relatively higher photocatalytic activity. As revealed from the SEM and TEM images, the Ag@AgCl was anchored on the surface of Bi_2WO_6. In this synthesis process, the Bi_2WO_6 sheets acted as an excellent substrate which efficiently prevented the aggregation of the Ag@AgCl. The narrow size distribution of the Ag@AgCl on the surface of Bi_2WO_6 could be ascribed to the effect of surfactant (CTAC) and microemulsion system on controlling the particle size and shape.

The optical absorption properties of the as-prepared samples were investigated by UV–vis spectrophotometry. The typical UV–vis diffuse reflection spectra of all samples show intense absorption bands with a steep edge in the visible light region, as shown in Fig. 4, which revealed that it is the band gap transition rather than the transition from impurity levels that were responsible for the visible light absorption band [25]. The Bi_2WO_6 sample possessed photo-absorption in both the UV and vis light regions up to 445 nm, which enhanced its visible light induced photocatalytic activity. The band gap was calculated according to the absorption edge to be approximately 2.79 eV. The absorption intensity of the prepared samples varied with varying Ag@AgCl loading amount. The Ag-loaded Bi_2WO_6 composites exhibited enhanced photo-absorption in the visible light region compared to pure Bi_2WO_6. In addition, the absorbance intensity of the P-Ag@AgCl (20 wt.%)/Bi_2WO_6 was lower than that of Ag@AgCl (20 wt.%)/Bi_2WO_6 synthesized via the oil-in-water self-assembly method. This suggest that the oil-in-water self-assembly procedure resulted in a uniform Ag@AgCl distribution on the surface of Bi_2WO_6 and decreased the resulting particle sizes of Ag@AgCl, which can also be confirmed by the SEM results (Fig. 2c and d). Meanwhile, a broad prominent absorption in the visible light region of 450–600 nm was observed in Ag@AgCl-based composites, which could be attributed to the surface plasmon resonance (SPR) effect of Ag [26–28]. The surface plasmon absorption on the surface of Ag derives from a collective oscillation of free electrons excited by the matching photon energy.

In order to determine the chemical composition of Ag@AgCl/Bi_2WO_6 and identify the chemical state of the Ag element in the samples, XPS characterization was performed. Fig. 5A is XPS survey spectra of Ag@AgCl (20 wt.%)/Bi_2WO_6. The Ag@AgCl/Bi_2WO_6 sample contains Ag, Cl, Bi, W, O and C elements. The emergence of the C element can be attributed to adventitious carbon from the sample fabrication and/or the XPS instrument itself [29]. Fig. 5B displays the Ag 3d level spectrum. The Ag 3d3/2 and Ag 3d5/2 spin–orbital photoelectrons were located at binding energies of 372.9 eV and 366.9 eV, respectively. The Ag 3d5/2 peak is further divided into two different peaks at 367.1 and 366.2 eV and the Ag 3d3/2 is also divided into two different peaks at 373.2 and 372.3 eV. According to the report [30] by Zhang et al., the peaks at 373.2 and 367.1 eV were attributed to metallic silver, and these two peaks with a spin energy separation of 6.1 eV further indicated that the Ag^0 existed in the Ag@AgCl/Bi_2WO_6 rectorite composite [31]. The Ag 3d peaks which appeared at the binding energies of 372.3 and 366.2 eV belonged to the Ag^+, indicating the formation of AgCl on the as-prepared photocatalyst [32]. These observations confirmed that Ag^+ ions were successfully reduced to metallic Ag via irradiation.

Fig. 6 shows the TEM images and UV–vis diffuse reflectance spectra of Ag@AgCl (20 wt.%)/Bi_2WO_6 with different photoreduction time: (a) 5 min, (b) 30 min, (c) 60 min. The series of Ag@AgCl (20 wt.%)/Bi_2WO_6 photocatalysts exhibited broad absorption in the about 430–780 nm region of visible light, owing to the surface plasmon resonance(SPR) effect of Ag NPs, which

Table 2
The major element content of photocatalysts.

Major element	Ag	Cl	Bi	W	O
Ag@AgCl (20 wt.)/Bi_2WO_6 (content, mass%)	11.97	3.01	46.95	21.62	14.01

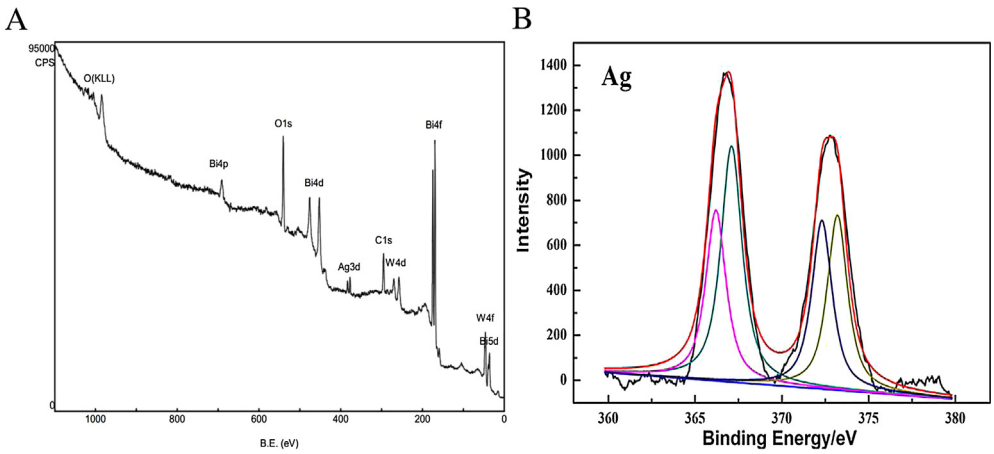

Fig. 5. XPS spectra of Ag@AgCl (20 wt.%)/Bi_2WO_6 photocatalys (A) survey spectrum; (B) Ag 3d.

were produced by the photo-reduction of AgCl. When the catalysts were irradiated with visible light, some Ag nanoparticles on the surface of the catalysts might become larger as a result of the reduction of AgCl [12]. Therefore, the diameters of the Ag@AgCl vary over a large range. As a result, the frequency of their plasmonic oscillations covers a wide range, permitting Ag@AgCl/Bi_2WO_6 to absorb visible and UV light over a wide range. The red-shift of absorption range suggests that the increase of Ag@AgCl diameters. As the duration of photo-reduction increased, Ag NP contents increased correspondingly [10], resulting in the enhanced intensity of visible light response from 5-Ag@AgCl (20 wt.%)/Bi_2WO_6 to 60-Ag@AgCl (20 wt.%)/Bi_2WO_6 and the larger diameters of the Ag@AgCl from about 10 nm (Fig. 6a) to 40 nm (Fig. 6c).

In order to probe into the photo-induced electron transfer in Ag@AgCl/Bi_2WO_6, time-resolved PL experiments were performed to evaluate the lifetimes [33] and then the PL decays for Bi_2WO_6 and Ag@AgCl (20 wt.%)/Bi_2WO_6 is shown in Fig. 7. The Bi_2WO_6 exhibit an instantaneous response near zero delay, which is well interpreted as correlation of laser pulse. The PL lifetime of Bi_2WO_6 was found to be about 0.3 ns. The addition of Ag@AgCl results in an efficient and complete PL quenching: an efficient PL quenching is indicative of a high degree of the photo-induced electron transfer in Ag@AgCl/Bi_2WO_6 [34]. This result suggested that migration rate of photo-generated charge carriers was fastest, which indicated that the composite exhibited efficient charge carrier separation.

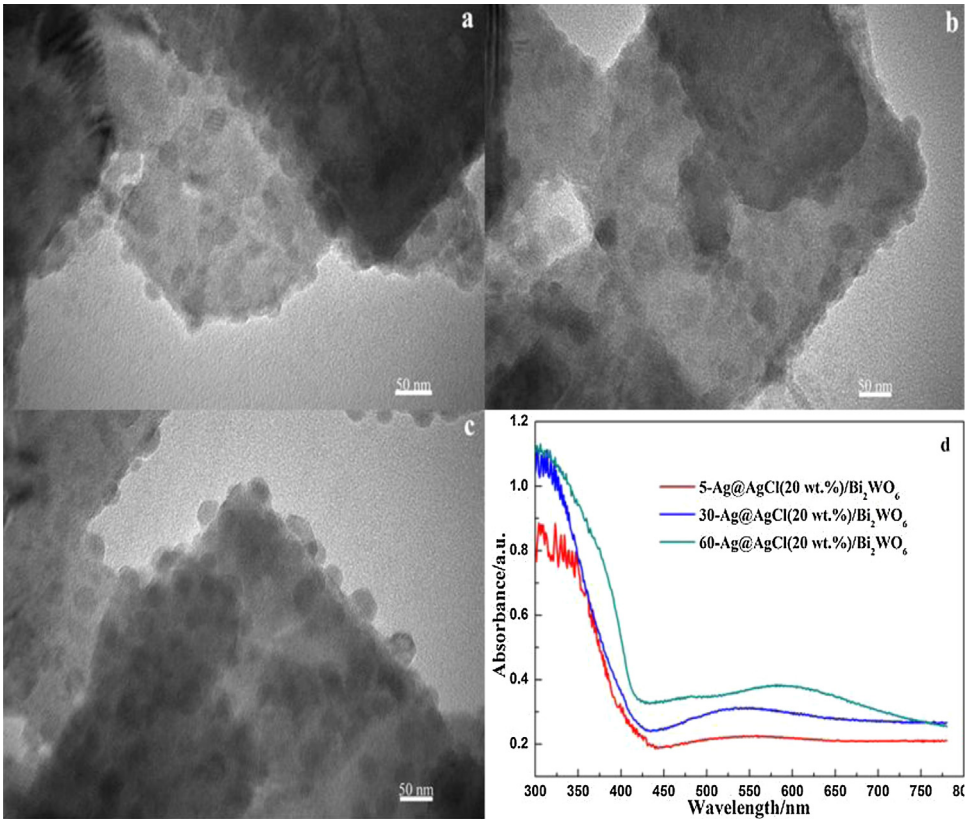

Fig. 6. TEM images and UV–vis diffuse reflectance spectra of Ag@AgCl (20 wt.%)/Bi_2WO_6 with different photo-reduction time prepared photocatalysts: (a) 5-Ag@AgCl (20 wt.%)/Bi_2WO_6, (b) 30-Ag@AgCl (20 wt.%)/Bi_2WO_6, (c) 60-Ag@AgCl (20 wt.%)/Bi_2WO_6.

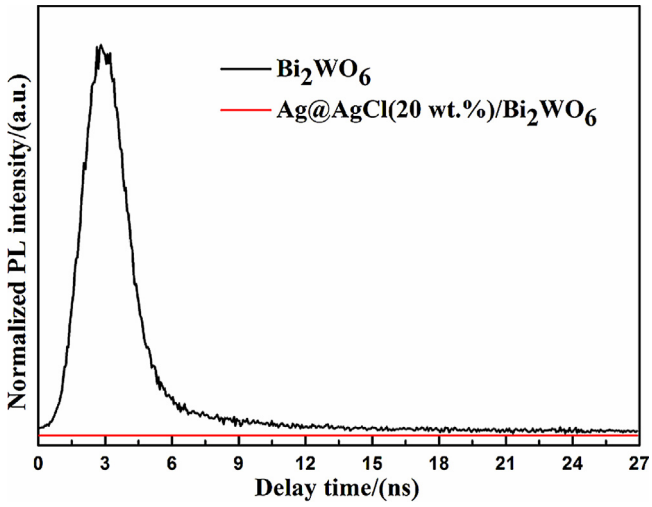

Fig. 7. Time-resolved PL spectrum of Bi_2WO_6 and Ag@AgCl (20 wt.%)/Bi_2WO_6 photocatalysts.

3.2. Photocatalytic activity

The photocatalytic degradation of RhB molecules was used to evaluate the photocatalytic activity of samples under visible light irradiation. As shown in Fig. 8, from the observed degradation, the blank test confirmed that RhB was only slightly degraded in the absence of catalyst, indicating that the photolytic degradation was negligible. In contrast, the Ag@AgCl/Bi_2WO_6 exhibited good photocatalytic degradation activity under visible light irradiation, degrading nearly 97.61% of RhB after 2 h irradiation. However, the same material prepared by precipitation degraded only 91.4% of RhB after irradiation for 2 h. The difference observed was thought to be attributed to the surface of the formed AgCl nanostructures being primarily terminated by and thus relatively enriched with Ag in the materials prepared via oil-in-water synthesis, resulting in their relatively higher photocatalytic activity. In addition, the oil-in-water self-assembly procedure resulted in a uniform Ag@AgCl distribution on the surface of Bi_2WO_6 and reduced the particle size of Ag@AgCl, providing more active sites. In contrast, the concentration of RhB remained almost unchanged in the dark controls for 2 h. Moreover, only 74.07% RhB was degraded by pure

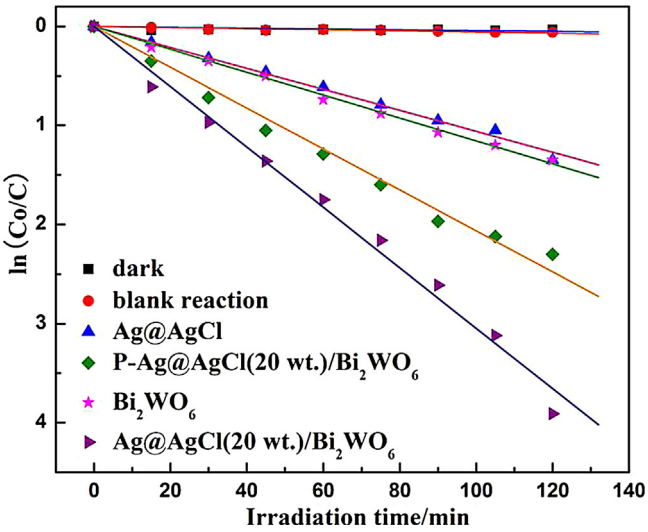

Fig. 8. Comparison of photocatalytic activities of various photocatalysts with the same weight.

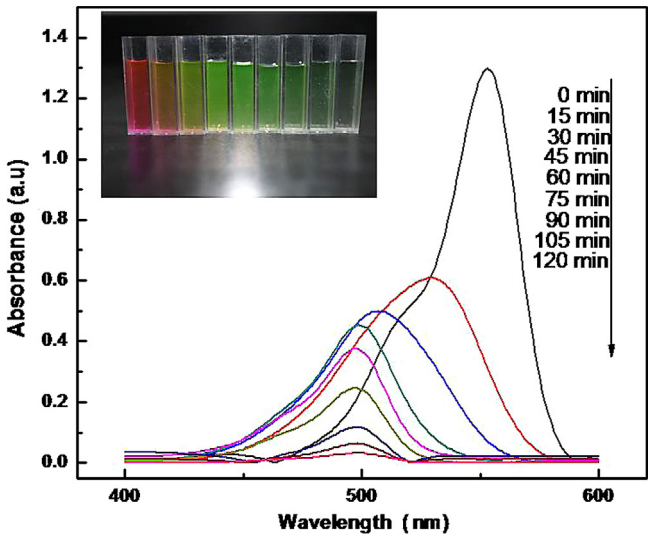

Fig. 9. Change in UV/vis absorption of RhB aqueous solutions under visible-light irradiation in the presence of Ag@AgCl (20 wt.%)/Bi_2WO_6 composite samples.

Bi_2WO_6 under visible light in 2 h. The RhB degradation ability of Ag@AgCl (calculated based on the equivalent Ag@AgCl content in Ag@AgCl/Bi_2WO_6) was also investigated using the same experimental conditions, and the degradation rate of Ag@AgCl/Bi_2WO_6 was observed to be higher than that of Ag@AgCl catalyst. According to our results, the photocatalytic activity of Bi_2WO_6 modified with Ag@AgCl had a significantly improved rate of RhB degradation compared to that of the pure Bi_2WO_6 material, and this improvement was thought to be due to the surface plasmon resonance enhancement of Ag NPs and the interaction between nano Ag@AgCl and Bi_2WO_6 [35]. The absorption changes for the RhB solution in the presence of Ag@AgCl (20 wt.%)/Bi_2WO_6 catalyst during the photocatalytic process are shown in Fig. 9. The spectral maximum peak was observed to shift from 554 to 498 nm due to *N*-deethylation and destruction of the conjugated structure [36], and the blue shift was similar to the report of Zhu [37] for the RhB/Bi_2WO_6 system. Under visible light irradiation, the dye was de-ethylated in a stepwise manner with the color of the dispersion changing from the initial red to a light green–yellow (as shown the inset of Fig. 9). Deethylation of the fully *N*,*N*,*N*′,*N*′-tetraethylated rhodamine molecule (RhB) is accompanied by a blue shift in the peak wavelength (552 nm). For example, *N*,*N*,*N*′-triethylated rhodamine is associated with a peak wavelength of 539 nm; *N*,*N*′-diethylated rhodamine, 522 nm; *N*-ethylated rhodamine, 510 nm; and rhodamine, 498 nm [38], respectively. RhB was thought to form Rhodamine after being fully demethylated, and further degradation of the molecule by photocatalysis occurred through destruction of the conjugated structure.

The photocatalytic degradation kinetic curve was investigated by the first-order simplification of Langmuir–Hinshelwood (L–H) kinetics, which is well established for photocatalysis at low initial pollutant concentrations [39]. The relevant equation is as follows:

$$\ln\frac{C_0}{C} = kt \quad (2)$$

where C_0/C is the ratio of the concentration of the dyes at adsorption–desorption equilibrium and after various intervals of time, and k is the apparent first-order rate constant (min^{-1}). The k value is obtained from the gradient of the graph of $\ln(C_0/C)$ versus time (t), which is shown in the insert of Fig. 10. The plots of irradiation time (t) versus the $\ln(C_0/C)$ displayed nearly linear trends for various amounts of Ag@AgCl doping contents from 5 to 25%, and the loading amounts were observed to strongly influence the activity obtained. The reaction rate constant k for the photocatalytic

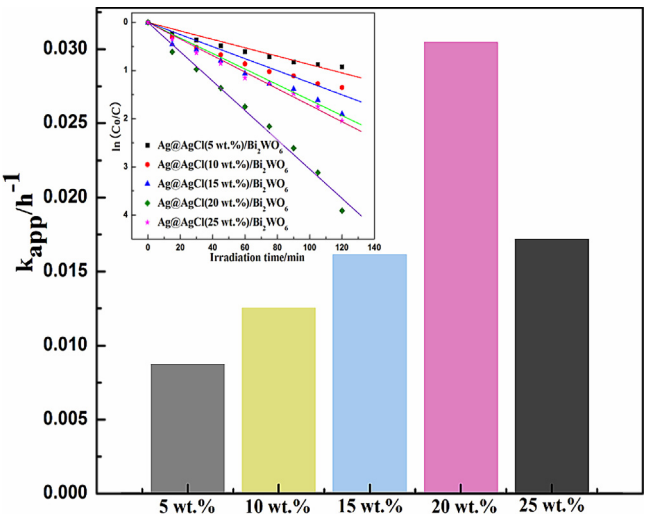

Fig. 10. First-order rate constant of (a) Ag@AgCl (5 wt.%)/Bi_2WO_6, (b) Ag@AgCl (10 wt.%)/Bi_2WO_6, (c) Ag@AgCl (15 wt.%)/Bi_2WO_6, (d) Ag@AgCl (20 wt.%)/Bi_2WO_6 and (e) Ag@AgCl (25 wt.%)/Bi_2WO_6.

degradation of RhB with Ag@AgCl/Bi_2WO_6 composites containing 5 wt.%, 10 wt.%, 15 wt.%, 20 wt.% and 25 wt.% Ag@AgCl was 0.0087, 0.0125, 0.0161, 0.0305 and 0.0172 h^{-1}, respectively. The sample prepared using a loading of 20 wt.% exhibited the highest photodegraded efficiency (0.0305 h^{-1}), and was thought to represent an optimal loading contributing to good particle dispersion and high photocatalytic activity. Once the loading of Ag@AgCl increased beyond a critical value, the nano-clusters of Ag@AgCl species were thought to agglomerate and shade the active sties on the surface of Bi_2WO_6, resulting in a lower degradation rates [40]. Therefore, an optimal Ag@AgCl loading amount on Bi_2WO_6 existed, and was found to be 20% in this study.

The electrons and holes produced by photocatalysis have strong reduction and oxidation abilities. However, they usually do not react with the organic dyes directly. Instead, some active species (such as •OH and $\bullet O_2^-$) are first formed through the reaction of charges and adsorbed H_2O or O_2 [41]. For various photocatalysts, the main active species may vary due to the differences in band structure or phase compositions. Therefore, different scavenges used as probes were introduced into the photocatalytic degradation of RhB in order to determine the relative roles of the reactive species. As shown in Fig. 11, EDTA was added as an h^+ scavenger to the reaction liquid, and L-ascorbic acid was used as an $\bullet O_2^-$ scavenger, while $NaHCO_3$ was used as an •OH radical scavenger. If the

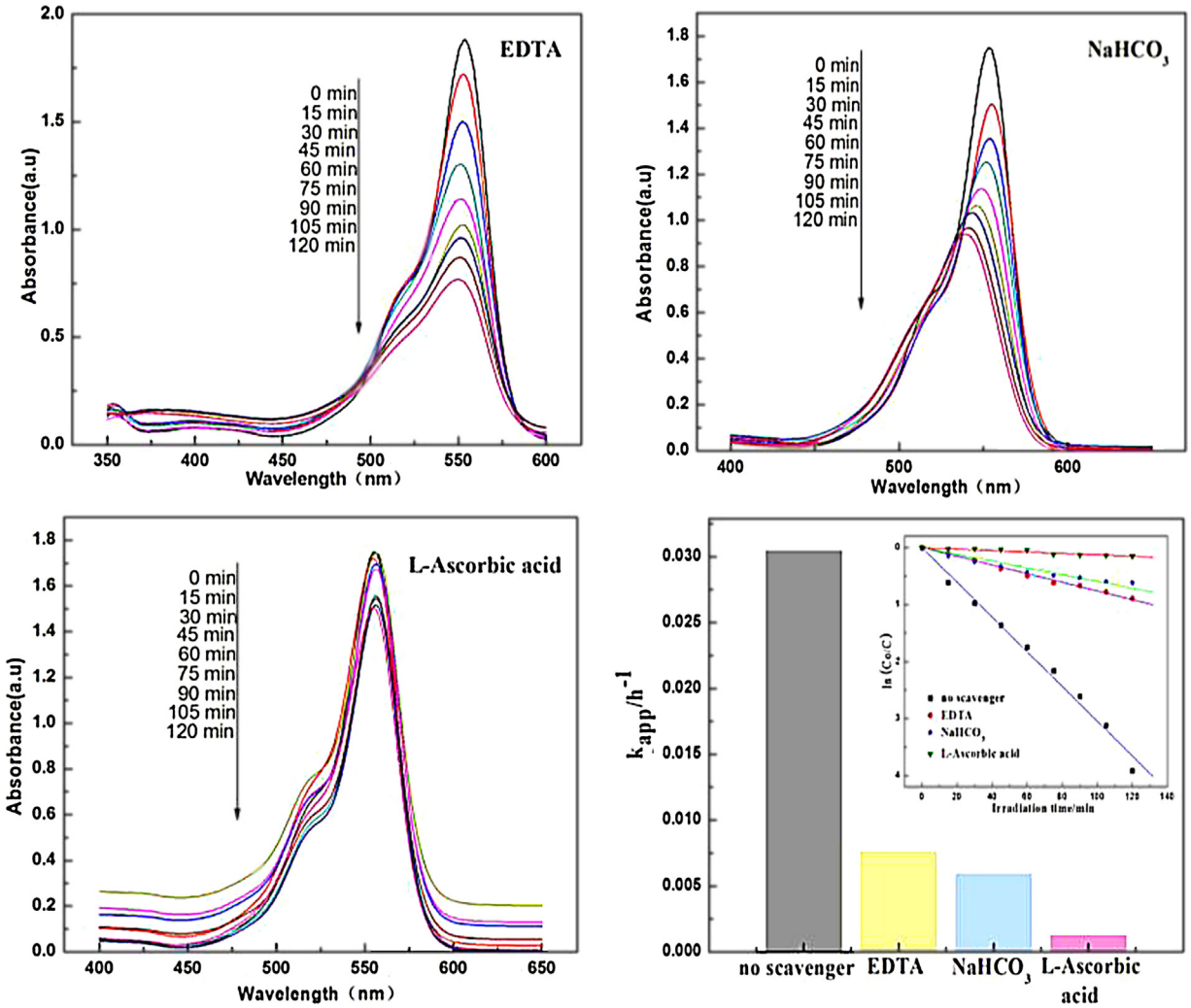

Fig. 11. Photocatalytic degradation of RhB with Ag@AgCl (20 wt.%)/Bi_2WO_6 in the presence of various scavengers under visible light. (a) EDTA, (b) $NaHCO_3$, (c) L-Ascorbic acid, and (d) comparison of the visible light photocatalytic activity obtained using rate constant k_{app}.

free radical scavenged played acted an important role in the photocatalytic degradation of RhB, the rate constant (k_{app}) would be reduced greatly in the presence of the appropriate scavenger. As seen in Fig. 11, the introduction of EDTA had a significant effect on the k_{app} compared to the runs performed in the absence of scavenger, suggesting that h^+ was a dominant reactive species. The degradation efficiency of RhB was also reduced significantly upon the introduction of L-ascorbic acid, indicating that $\bullet O_2^-$ also played a large role in the photocatalytic degradation process. However, the suppression by L-ascorbic acid on photocatalytic activity was not so great, and it was thought that another important reactive species might affect the activity observed. Considering that the accumulated holes could oxidize Cl^- to Cl^0, it was thought that Cl^0 atoms were the active species and participated in the degradation of RhB [42,43]. The phenomenon that the h^+ show a negligible effect on the reaction of RhB would be explained by this inference [44]. In addition, the use of $NaHCO_3$ as a scavenger had a positive effect on the k_{app} of RhB degradation compared to the runs performed in the absence of scavenger, suggesting that •OH was a major free radical. However, the standard redox potential of Bi^V/Bi^{III} is more negative than that of $\bullet OH/OH^-$ (+1.99), suggesting that the hole photo-generated on the surface of Bi_2WO_6 could not react with OH^-/H_2O to form •OH [25]. The result could be verified by terephthalic acid photoluminescence (TA-PL) probing technique [45] to further detect the formation of •OH. Additionally, as it is well known, the photocatalytic degradation of RhB can occur by two competitive mechanisms [46]: by attacking •OH radicals on the aromatic chromophore ring, leading to the degradation of the RhB structure and reduction of the absorption band without a wavelength shift (pathway 1) or by a successive de-ethylation from the aromatic rings, causing significant blue wavelength shifts according to the formation of the different de-ethylated rhodamine intermediates (pathway 2). The UV/vis absorption for the RhB solution in the presence of Ag@AgCl/Bi_2WO_6 catalyst shows blue shift by pathway 2. But the blue shift of UV/vis absorption of RhB did not happen when some scavengers were added in the system as shown. The main RhB absorption band located at 554 nm is due to the presence of four ethylated groups on the dye molecule. The degradation pathway changed due to lack of some active species (such as h^+ and $\bullet O_2^-$) when some scavengers were added during the RhB photocatalytic degradation. This is an important point because a complete RhB mineralization leads to the bleaching of the solution, but not necessarily to the de-ethylation of the dye.

The stability of the photocatalytic performance of the Ag@AgCl/Bi_2WO_6 catalyst, which is an important factor in practical applications, was evaluated. The recycling runs of the photocatalytic degradation of RhB by the Ag@AgCl (20 wt.%)/Bi_2WO_6 sample under visible-light were studied (Fig. 12). The efficiency decreased from 97.61% in the 1st run to 89.11% in the 5th run, and this decrease was thought to be due to some catalyst washout during the recovery steps, which could be minimized through the use of centrifugation between runs. However, the acceptable activity in repeated uses indicated the excellent stability of Ag@AgCl/Bi_2WO_6 catalyst and suggested the Ag@AgCl nanoparticles were firmly connected to the Bi_2WO_6 nanosheets [47]. Therefore, the results obtained illustrate that the incorporation of Ag@AgCl into the Bi_2WO_6 matrix not only enhances the visible light photocatalytic performance of Bi_2WO_6, but also inhibits the photo-corrosion, thus giving rise to a stable durability of photocatalytic activity [45].

Phenol is a colorless organic compound and was also chosen as a model contaminant. In order to evaluate the photocatalytic activity of Ag@AgCl/Bi_2WO_6, the degradation of phenol was studied under various conditions, to assess the effect of photocatalysis on the overall degradation rate for an initial concentration of 5 mg/L with 150 mL, as shown in Fig. 13. The experimental results obtained indicated that the concentration of phenol was almost

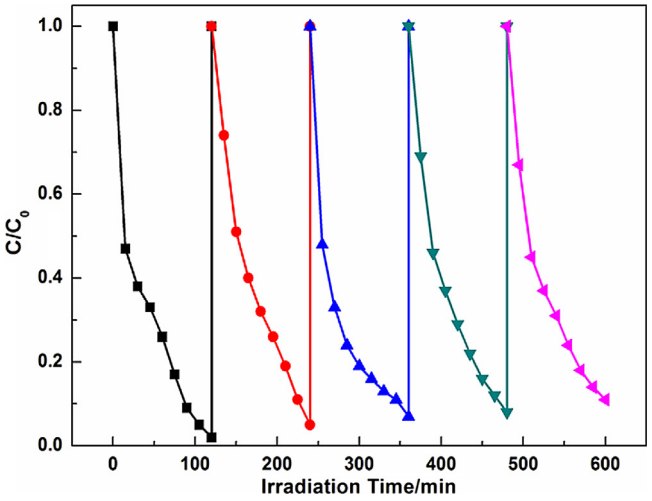

Fig. 12. Cycling runs for photocatalytic degradation of RhB over the Ag@AgCl (20 wt.%)/Bi_2WO_6 photocatalyst under visible light irradiation. Experimental condition: RhB concentration (10 mg/L, 250 mL), catalyst concentration (1 g/L).

unchanged in the dark controls for 2 h, and the blank test confirmed that phenol could not be degraded significantly under irradiation, indicating that the photolysis can be ignored. The phenol degradation rates were 69%, 45% and 37% over Ag@AgCl/Bi_2WO_6, pure Ag@AgCl and Bi_2WO_6, respectively, under visible light. By comparison of the phenol degradation rates, the photocatalytic activity of Ag@AgCl/Bi_2WO_6 was confirmed for the degradation of phenol, and affirmed that the disappearance of phenol molecules was due to photocatalytic degradation instead of only to adsorption.

It was widely known that the separation efficiency of electrons and holes plays a vital role in the photocatalytic reaction [48]. Photocurrent can be produced from the photo-generated electrons in the conducting bands of semiconductor photocatalysts with leaving holes in their valence bands. Therefore, higher photocurrents are indicative of better electron and hole separation efficiencies, and thus higher photocatalytic activities [49]. The photoelectrochemical properties of the pure Bi_2WO_6 and Ag@AgCl/Bi_2WO_6 electrodes were measured in Na_2SO_4 electrolyte under visible light irradiation. The plots of the transient photocurrent responses of the pure Bi_2WO_6 and Ag@AgCl/Bi_2WO_6 composite with 10 wt.% and 20 wt.% Ag@AgCl versus time were recorded for several on–off cycles of visible light irradiation, as shown in Fig. 14. As seen, the dark current was very low, and was drastically increased when the irradiation was turned on. The photocurrent returned to the original value as soon as the illumination of light on the photoanode was stopped. This indicated that the photocurrent of the system was mostly due to the photocurrent produced by the illumination of light on the photo-anode. Moreover, the photocurrent density is 6.2, 5.3 and 1.2 $\mu A/cm^2$ for Ag@AgCl (20 wt.%)/Bi_2WO_6, Ag@AgCl (10 wt.%)/Bi_2WO_6 and Bi_2WO_6 electrodes, respectively. The Ag@AgCl/Bi_2WO_6 electrode showed a considerably enhanced photocurrent density compared with the pure Bi_2WO_6 electrode, indicating that the Ag@AgCl loading promoted the transfer of the photo-generated electrons–holes and inhibited the rapid recombination of photo-charges. Therefore, Ag@AgCl/Bi_2WO_6 should predictably exhibit an improved photocatalytic activity for organic pollutant degradation.

As a powerful tool to explore the electrochemical process, EIS has been widely employed in testing the electro-catalytic activity for the regeneration of a redox couple [50]. Fig. 15 shows the Nyquist plots of the as prepared Bi_2WO_6 and Ag@AgCl/Bi_2WO_6 under visible-light irradiation. Based on corresponding equivalent electrical circuit (inset of Fig. 15), impedance spectra were fitted

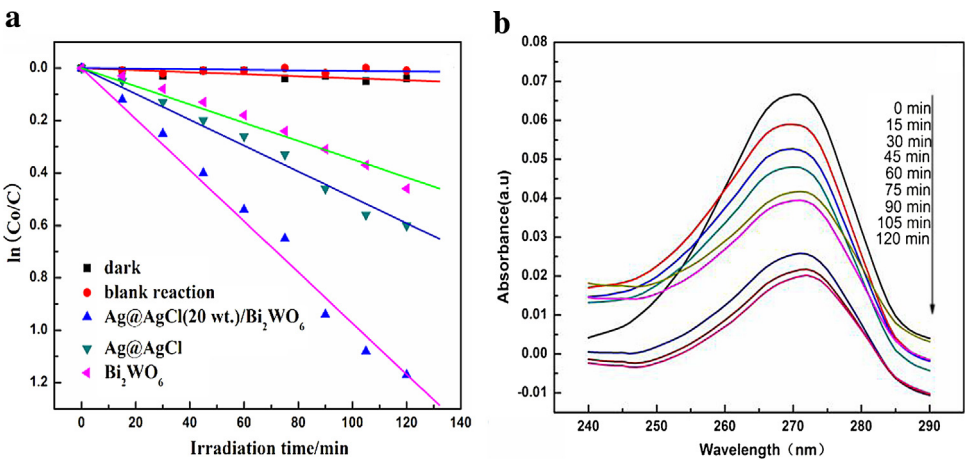

Fig. 13. (a)Concentration change of phenol over Ag@AgCl, Bi_2WO_6 and Ag@AgCl/Bi_2WO_6 samples under visible light irradation. Experimental conditions: phenol concentration (5 mg/L, 150 mL), catalyst concentration (1 g/L) (b) Temporal UV–vis absorption spectral changes during the photocatalytic degration of phenol in aqueous solution.

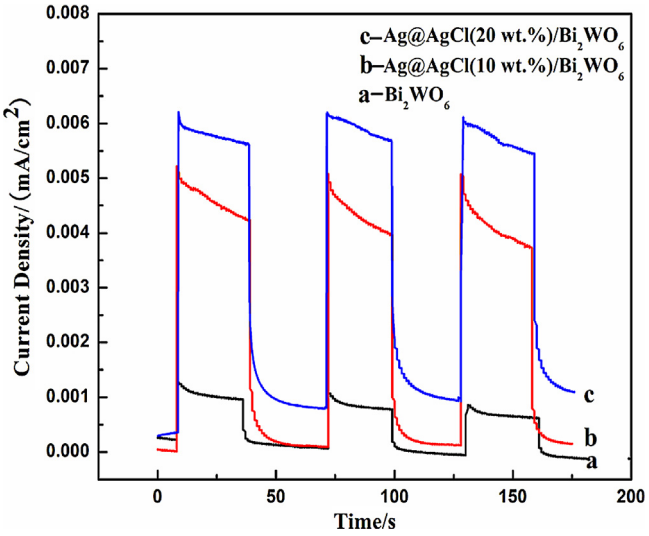

Fig. 14. Transient photocurrent of Bi_2WO_6 and Ag@AgCl/Bi_2WO_6 under visible light irradiation.

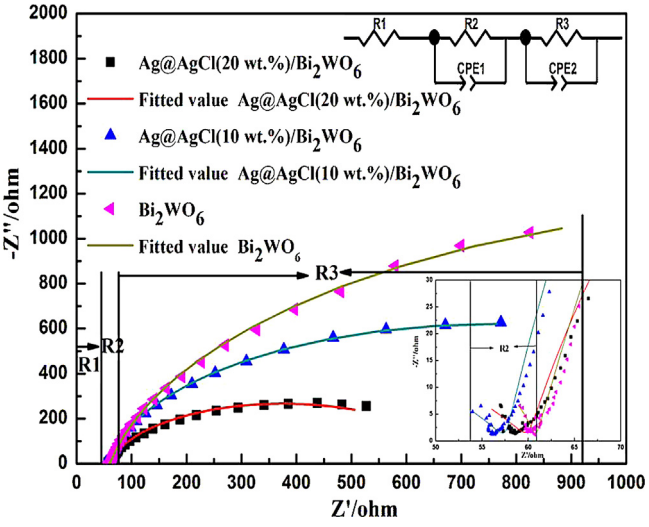

Fig. 15. The electrochemistry properties of Bi_2WO_6 and Ag@AgCl/Bi_2WO_6 electrodes under visible light irradiation: impedance spectra with the corresponding equivalent circuit models.

by the ZsimpWin software and a series of circuit parameters were obtained. In the impedance spectroscopy, the intercept on the real axis (high frequency) can be attributed to the series resistance (R1) of Pt counter electrode. The first semi-circle (high frequency) can be assigned to the charge-transfer resistance (R2) of the Pt counter electrode/electrolyte interface. The second semi-circle (middle frequency,) can be assigned to the charge-transfer resistance (R2) of the as prepared samples anode/electrolyte interface. Moreover, one imperfect semicircular arc in the low frequency range represented the electrode interface diffusion [51]. The radius of the arc on the EIS Nynquist plot reflects the reaction rate occurring at the surface of electrode. The arc radius on EIS Nynquist plot of Bi_2WO_6 was smaller than that of Ag@AgCl/Bi_2WO_6 sample, which meant that an effective separation of photo-generated electron–hole pairs and fast interfacial charge transfer to the electron donor/electron acceptor occurred as suggested [52].

4. Photocatalytic degradation mechanism under visible light

To further understand the mechanism for the enhanced photocatalytic performance of the Ag@AgCl/Bi_2WO_6 photocatalysts, the materials were analyzed considering the following perspectives. A plasmonic Z-scheme mechanism of Ag@AgCl/Bi_2WO_6 composite nanoplates was proposed [25,53] and shown in Fig. 16. The existence of Ag@AgCl nanocrystals on the surfaces of the Bi_2WO_6 formed a uniquely hierarchical nanostructure, which provided a high surface area and a large number of interfaces between the Ag@AgCl and Bi_2WO_6 species. The high surface areas and large number of interfaces accessible to the outer environment were thought to provide numerous active sites for the photocatalytic degradation of dye molecules. The band gaps of Bi_2WO_6 and AgCl are 2.79 eV and 3.25 eV, respectively. The metallic Ag clusters formed in situ on the AgCl semiconductor were thought to enhance the absorption in the visible light region due to the surface plasmon resonance effect. Under visible-light irradiation, both Ag nanoparticles and Bi_2WO_6 can absorb visible-light photons to produce photo-generated electrons and holes. The plasmon-induced electrons of Ag nanoparticles are injected into the CB of AgCl to reduce oxygen, while the holes remain on the Ag nanoparticles. For Bi_2WO_6 [54–56], the photo-generated electrons excited to the conduction band of Bi_2WO_6 under visible light irradiation were entrapped by Ag nanoparticles to recombine with the plasmon-induced holes [57] produced by plasmonic absorption of Ag nanoparticles due to its high Schottky barrier at the metal–semiconductor interface,

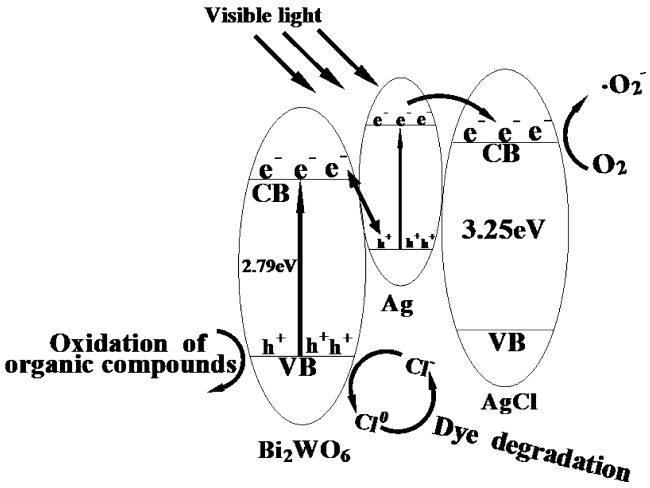

Fig. 16. Schematic diagram of the photocatalytic mechanism of Bi_2WO_6 loaded with Ag@AgCl.

while the VB holes remain on Bi_2WO_6 to oxidize organic substances. In addition, due to the existence of Cl^- ions in the reaction solution [58], the standard redox potential of Cl^-/Cl^0 (1.36 eV) is more negative than that E_{VB} of Bi_2WO_6 (+3.26 eV) [59], suggesting that a part of the holes generated on Bi_2WO_6 worked to oxidize Cl^- ions to Cl^0 atoms [60,61]. The Cl^0 atoms, in turn, acted as reactive species for the oxidation of dye molecules. The plasmon-induced electrons of the CB of AgCl were thought to be trapped by absorbed O_2 to produce $\bullet O_2^-$, which could oxidize RhB and result in a high photocatalytic degradation rate. Furthermore, Ag/AgCl nanoparticles loaded on the Bi_2WO_6 could also act independently as superior visible-light-driven photocatalysts for degrading organic contaminants, further enhancing the photocatalytic activity of the Ag@AgCl/Bi_2WO_6 composite

5. Conclusions

Ag@AgCl/Bi_2WO_6 hierarchical composites were successfully prepared by a facile oil/water self-assembly method with flower-like Bi_2WO_6 samples as substrates. The Bi_2WO_6 particles possessed orthorhombic structures, even upon sensitization with QDs Ag@AgCl. The photocatalytic experimental results indicated that the Ag@AgCl/Bi_2WO_6 composites exhibited much higher visible-light-driven catalytic activity than pure Bi_2WO_6. In addition, the appropriate loading content of QDs Ag@AgCl on the composite efficiently enhanced the photocatalytic degradation rate and the Ag@AgCl (20 wt.)/Bi_2WO_6 composite was found to exhibit the best photocatalytic activity for the degradation of RhB. The enhanced photocatalytic activity was attributed to the increased surface area, tight interface contact which could improve the photo-induced charge separation after QDs Ag@AgCl coupled with flower-like Bi_2WO_6. Meanwhile, due to the surface plasmonic resonance (SPR) of Ag nanoparticles and the light scattering effect of flower-like structure Bi_2WO_6, Ag@AgCl/Bi_2WO_6 composites exhibited excellent UV–vis absorption, resulting in a relatively higher photocatalytic activity. In addition, the oil-in-water self-assembly procedure resulted in a uniform Ag@AgCl distribution on the surface of Bi_2WO_6 and reduced the particle size of Ag@AgCl to provide more active sites. Besides the excellent photocatalytic activity, Ag@AgCl/Bi_2WO_6 also possessed good stability in cyclic photocatalysis trials. Detailed electrochemical characterizations showed that the Ag@AgCl (20 wt.%)/Bi_2WO_6 electrode exhibited a high specific photocurrent of 6.2 $\mu A/cm^2$. A mechanism for the increased activity in Ag@AgCl/Bi_2WO_6 system was proposed, and the synthesis method used to prepare this material was thought to be useful in the further design and synthesis of novel high-performance photocatalysts. The Ag@AgCl/Bi_2WO_6 photocatalyst synthesized possessed excellent activity and stability, and holds potential for future research on coupled photocatalysts and their practical application in environmental purification.

Acknowledgements

This work was supported by the National Natural Science Foundation of China (grant nos. 51172063, 51202056, 51372068), Hebei Natural Science Funds for Distinguished Young Scholar (grant no. B2014209304), Hebei Natural Science Funds for the Joint Research of Iron and Steel (grant no. B2014209314), Hebei Provincial Foundation for Returned Scholars. Yinghua Liang and Shuanglong Lin both contributed equally to this work.

References

[1] F. Zhou, R. Shi, Y.F. Zhu, J. Mol. Catal. A: Chem. 340 (2011) 77–82.
[2] R. Asahi, T. Morikawa, T. Ohwaki, K. Aoki, Y. Taga, Science 293 (2001) 269–271.
[3] J. Zhu, J. Ren, Y.N. Huo, Z.F. Bian, H.X. Li, J. Phys. Chem. C 51 (111) (2007) 18965–18969.
[4] M. Hara, T. Kondo, M. Komoda, S. Ikeda, K. Shinohara, A. Tanaka, J.N. Kondo, K. Domen, Chem. Commun. 357 (1998) 357–358.
[5] W.F. Shangguan, A. Yoshida, J. Phys. Chem. B 47 (106) (2002) 12227–12230.
[6] A. Kudo, K. Omori, H. Kato, J. Am. Chem. Soc 49 (121) (1999) 11459–11467.
[7] M. Pastore, F.D. Angelis, Phys. Chem. Chem. Phys. 14 (2012) 920–928.
[8] L.S. Zhang, K.H. Wong, Z.G. Chen, J.C. Yu, J.C. Zhao, C. Hu, C.Y. Chan, P.K. Wong, Appl. Catal., A: Gen. 363 (2009) 221–229.
[9] Y.Y. Li, Y. Ding, Phys. Chem. C 114 (2010) 3175–3179.
[10] B.W. Ma, J.F. Guo, W.L. Dai, K.N. Fan, Appl. Catal., B: Environ. 123–124 (2012) 193–199.
[11] S. Sohrabnezhada, A. Pourahmad, Spectrochim. Acta, A: Mol. Biomol. Spectrosc. 86 (2012) 271–275.
[12] J.F. Guo, B.W. Ma, A.Y. Yin, K.N. Fan, W.L. Dai, J. Hazard. Mater. 211–212 (2012) 77–82.
[13] C. Hu, T.W. Peng, X.X. Hu, Y.L. Nie, X.F. Zhou, J.H. Qu, H. He, J. Am. Chem. Soc. 2 (132) (2010) 857–862.
[14] Y.L. Min, G.Q. He, Q.J. Xu, Y.C. Chen, J. Mater. Chem. A 2 (2014) 1294–1301.
[15] C. Hu, J. Guo, J.H. Qu, X.X. Hu, Langmuir 9 (23) (2007) 4982–4987.
[16] H.F. Cheng, B.B. Huang, P. Wang, Z.Y. Wang, Z.Z. Lou, J.P. Wang, X.Y. Qin, X.Y. Zhang, Y. Dai, Chem. Commun. 47 (2011) 7054–7056.
[17] L. Ge, J. Liu, Appl. Catal., B: Environ. 105 (2011) 289–297.
[18] Y.L. Lee, C.F. Chi, S.Y. Liau, Chem. Mater. 3 (22) (2010) 922–927.
[19] X.F. Gao, H.B. Li, W.T. Sun, Q. Chen, F.Q. Tang, L.M. Peng, J. Phys. Chem. C 18 (113) (2009) 7531–7535.
[20] X.N. Li, R.K. Huang, Y.H. Hu, Y.J. Chen, W.J. Liu, R.S. Yuan, Z.H. Li, Inorg. Chem. 51 (2012) 6245–6250.
[21] G.Y. Zhang, Y. Feng, Q.S. Wu, Y.Y. Xu, D.Z. Gao, Mater. Res. Bull. 47 (2012) 1919–1924.
[22] J.B. Zhou, Y. Cheng, J.G. Yu, J. Photochem. Photobiol., A: Chem. 223 (2011) 82–87.
[23] J.C. Yu, J. Guo, W. Kei, Z. Tao, L. Zhi, J. Mater. Chem. 14 (2002) 3808–3816.
[24] Y.F. Qiu, P.L. Chen, M.H. Liu, J. Am. Chem. Soc. 132 (2010) 9644–9652.
[25] H.B. Fu, C.S. Pan, W.Q. Yao, Y.F. Zhu, J. Phys. Chem. B 109 (2005) 22432–22439.
[26] B. Wiley, Y.G. Sun, B. Mayers, Y.N. Xia, Chem. Eur. J 11 (2005) 454–463.
[27] Y.X. Tang, P.X. Wee, Y.K. Lai, X.P. Wang, D.G. Gong, P.D. Kanhere, T.T. Lim, Z.L. Dong, Z. Chen, J. Phys. Chem. C 116 (2012) 2772–2780.
[28] M.R. Elahifard, S. Rahimnejad, S. Haghighi, M.R. Gholami, J. Am. Chem. Soc. 129 (31) (2007) 9552–9553.
[29] M.Y. Wang, L. Sun, Z.Q. Lin, J.H. Cai, K.P. Xie, C.J. Lin, Energy Environ. Sci. 6 (2013) 1211–1220.
[30] H. Zhang, G. Wang, D. Chen, X.J. Lv, J.H. Li, Chem. Mater. 20 (2008) 6543–6549.
[31] D.S. Wang, Y.D. Duan, Q.Z. Luo, X.Y. Li, L.L. Bao, Desalination 270 (2011) 174–180.
[32] Y.Q. Yang, G.K. Zhang, W. Xu, J. Colloid Interface Sci. 376 (2012) 217–223.
[33] Q.H. Li, X. Jin, X.W. Yang, C.Y. Chen, Z.H. Chen, Y.C. Qin, T.H. Wei, W.F. Sun, Appl. Catal., B: Environ. 162 (2015) 524–531.
[34] Q.H. Li, X. Jin, X.W. Yang, C.Y. Chen, Z.H. Chen, Y.C. Qin, T.H. Wei, W.F. Sun, Appl. Catal., B: Environ. 162 (2015) 524–531.
[35] P. Wang, B.B. Huang, X.Y. Zhang, X.Y. Qin, H. Jin, Y. Dai, Z.Y. Wang, J.Y. Wei, J. Zhan, S.Y. Wang, J.P. Wang, M.H. Whangbo, Chem. Eur. J. 15 (2009) 12576–12579.
[36] T.X. Wu, G.M. Liu, J.C. Zhao, H. Hidaka, N. Serpone, J. Phys. Chem. B 102 (1998) 5845–5851.
[37] C. Zhang, Y.F. Zhu, Chem. Mater. 17 (2005) 3537–3545.
[38] T. Watanabe, T. Takizawa, K. Honda, J. Phys. Chem. 19 (81) (1977) 1845–1851.
[39] D. Sarkar, U.N. Maiti, C.K. Ghosh, K.K. Chattopadhyay, Adv. Sci. Lett. 6 (2012) 127–133.
[40] J.D. Zhuang, W.X. Dai, P. Liu, Langmuir 26 (2010) 9686–9694.

[41] T.T. Li, Y.M. He, H.J. Lin, J. Cai, L.Z. Dong, X.X. Wang, M.F. Luo, L.H. Zhao, X.D. Yi, W.Z. Weng, Appl. Catal., B: Environ. 138–139 (2013) 95–103.
[42] J. Cao, B.Y. Xu, H.L. Lin, B.D. Luo, S.F. Chen, Chem. Eng. J. 185–186 (185) (2012) 91–100.
[43] Z.J. Zhou, M.C. Long, W.M. Cai, J. Cai, J. Mol. Catal. A: Chem. 353–354 (2012) 22–28.
[44] Q. Xiao, Z.C. Si, J. Zhang, C. Xiao, X.K. Tan, J. Hazard. Mater. 150 (2008) 62–67.
[45] N. Zhang, S.Q. Liu, X.Z. Fu, Y.J. Xu, J. Phys. Chem. C 115 (2011) 9136–9145.
[46] A. Martínez-de la Cruz, U.M. GarcíaPérez., Mater. Res. Bull. 45 (2010) 135–141.
[47] J.H. Xu, W.Z. Wang, S.M. Sun, L. Wang, Appl. Catal., B: Environ. 111–112 (2012) 126–132.
[48] J. Jiang, X. Zhang, P.B. Sun, L.Z. Zhang, J. Phys. Chem. C 115 (2011) 20555–20564.
[49] Q.J. Xiang, J.G. Yu, M. Jaroniec, J. Phys. Chem. C 115 (2011) 7355–7363.
[50] Q.H. Li, Q.W. Tang, N. Du, Y.C. Qin, J. Xiao, B.L. He, H.Y. Chen, L. Chu, J. Power Sources 248 (2014) 816–821.
[51] L. Wang, B.X. Han, L. Dai, H.Z. Zhou, Y.H. Li, Y.L. Wu, J. Zhu, J. Hazard. Mater. 262 (2013) 545–553.
[52] W.H. Leng, Z. Zhang, J.Q. Zhang, C.N. Cao, J. Phys. Chem. B 109 (2005) 15008–15023.
[53] X.F. Wang, S.F. Li, Y.Q. Ma, H.G. Yu, J.G. Yu, J. Phys. Chem. C 115 (2011) 14648–14655.
[54] J. Ren, W.z. Wang, S.m. Sun, L. Zhang, J. Chang, Appl. Catal., B: Environ. 92 (2009) 50–55.
[55] H.G. Yu, R. Liu, X.F. Wang, P. Wang, J.g. Yu, Appl. Catal., B: Environ. 111–112 (2012) 326–333.
[56] L.S. Zhang, H.L. Wang, Z.G. Chen, P.K. Wong, J.S. Liu, Appl. Catal., B: Environ. 106 (2011) 1–13.
[57] X.F. Wang, S.F. Li, Y.Q. Ma, H.G. Yu, J.G. Yu, J. Phys. Chem. C 115 (2011) 114648–114655.
[58] Y. Nakajima, Q.L. Jin, H. Tada, Electrochem. Commun. 10 (2008) 1132–1135.
[59] Y.L. Tian, B.B. Chang, J.L. Lu, J. Fu, F.N. Xi, X.P. Dong, ACS Appl. Mater. Interfaces 5 (2013) 7079–7085.
[60] H.J. Yan, S.J.T. Kochuveedu, L.N. Quan, S.S. Lee, D.H. Kim, J. Alloys Compd. 560 (2013) 20–26.
[61] R.F. Dong, B.Z. Tian, C.Y. Zeng, T.Y. Li, T.T. Wang, J.L. Zhang, J. Phys. Chem. C 117 (2013) 213–220.